Geoderma 239–240 (2015) 195–205

Contents lists available at ScienceDirect

Geoderma

journal homepage: www.elsevier.com/locate/geoderma

Extensive middle Miocene weathering interpreted from a well-preserved paleosol, Cricket Flat, Oregon, USA

Nicholas E. Bader [a,*], Kirsten P. Nicolaysen [a], Ricardo Lopez-Maldonado [b,1], Kira E. Murray [a,2], Anna C. Mudd [c,3]

[a] Department of Geology, Whitman College, 345 Boyer Ave., Walla Walla, WA 99362, USA
[b] Department of Geological Sciences, University of Idaho, 875 Perimeter Drive, Moscow, ID 83844, USA
[c] Department of Geology, The College of Wooster, 1189 Beall Ave., Wooster, OH 44691, USA

ARTICLE INFO

Article history:
Received 24 July 2014
Received in revised form 2 October 2014
Accepted 11 October 2014
Available online 29 October 2014

ABSTRACT

The high-resolution marine isotope climate record indicates pronounced global cooling during the Langhian (16–13.8 Ma), beginning with the warm middle Miocene climatic optimum and ending with significant Antarctic ice sheet expansion and the transition to "icehouse" conditions. However, the timing and rate of cooling during the Langhian are uncertain. Terrestrial paleoclimate data from this interval is sparse and sometimes conflicting; in particular, there are gaps in the terrestrial record in the Pacific Northwest during the late Langhian and early Serravallian between about 14.5 and 12.5 Ma. New terrestrial paleoclimate data from this time and region could help reconcile these conflicting records. Paleosols are particularly useful for reconstructing paleoenvironment because the rate and style of pedogenesis are primarily a function of surface environmental conditions; however, complete and well-preserved paleosols are uncommon. Most soils form in erosive environments that are not preserved, or in environments such as floodplains that accumulate in small increments; the resulting cumulic soils are usually thin, weakly developed, and subject to diagenetic overprinting from subsequent soils. The paleosol at Cricket Flat in northeastern Oregon is an unusually complete and well-preserved paleosol from a middle Miocene volcanic sequence in the Powder River Volcanic Field. An olivine basalt flow buried the paleosol at approximately 13.8 ± 0.6 Ma, based on three $^{40}Ar/^{39}Ar$ dates on the basalt. We described the Cricket Flat paleosol and used its physical and chemical profile and micromorphology to assess pedogenesis. The Cricket Flat paleosol is an Ultisol-like paleosol, chemically consistent with a high degree of weathering. Temperature and rainfall proxies suggest that Cricket Flat received 1120 ± 180 mm precipitation $year^{-1}$ and experienced a mean annual temperature of 14.5 ± 2.1 °C during the formation of the paleosol, significantly warmer and wetter than today. This suggests slower cooling after the middle Miocene climatic optimum than is seen in the existing paleosol record.

1. Introduction

Paleosols, beyond their value for understanding pedogenesis in general, can augment the terrestrial paleoclimate record. The terrestrial paleoclimate record provides a valuable window into Earth's climate system and its response to perturbations. The middle Miocene is especially interesting because it marks a major cooling period in Earth's history. The 17–15 Ma middle Miocene climatic optimum (MMCO) was a significant global greenhouse interval with marine and terrestrial indicators of warm and wet conditions (Sheldon, 2006), but by 13.8 Ma Earth had transitioned to an "icehouse" climate marking the beginning of the current ice age and major Antarctic ice sheet expansion (Holbourn et al., 2005).

Missing intervals in our proxy records obscure the details and timing of middle Miocene climate change. Marine sedimentary sequences record high-resolution climate records, primarily through $\delta^{18}O$ and $\delta^{13}C$ of benthic foraminifera (Holbourn et al., 2007; Zachos et al., 2001), but terrestrial climate records remain necessarily less complete due to interruptions in deposition and preservation. Terrestrial climate during this period is best known from fossil floras (Graham, 1999), analysis of leaf morphology (e.g., Yang et al., 2007; Wolfe, 1993), and indirectly through estimation of atmospheric pCO_2 calculated from the stomatal index of fossil leaves (Retallack, 2001). These records are valuable but sparse, as the conditions necessary for preserving the cell walls of fossil leaves are restricted to anoxic environments such as swamps and lake bottoms (Greenwood, 1991).

Paleosols can help us to reconstruct terrestrial paleoclimate because soils form from parent material by pedogenic processes that depend on conditions at Earth's surface (e.g., precipitation and heat flux) during

* Corresponding author.
E-mail address: baderne@whitman.edu (N.E. Bader).
[1] Present address: Department of Geosciences and Environment, California State University Los Angeles, 5151 State University Drive, Los Angeles, CA 90032, USA.
[2] Present address: Freestone Environmental Services, 1100 Jadwin Ave, Richland, WA 99352, USA.
[3] Present address: P.O. Box 245, Grass Valley, CA 95945, USA.

http://dx.doi.org/10.1016/j.geoderma.2014.10.007
0016-7061/

the time of soil formation (Sheldon and Tabor, 2009). Retallack (2007) compiled a terrestrial climate record using paleosols of eastern Oregon, Montana and Idaho, and the Great Plains, but certain intervals of this compilation lack datable paleosols, particularly the period after 14 Ma near the Langhian–Serravallian transition. For example, in eastern Oregon, the Mascall Formation contains numerous paleosols but spans 16–14.7 Ma (Bestland et al., 2008). Another sequence of paleosols developed on Picture Gorge Basalt flows spans 16–15.4 Ma (Sheldon, 2006). In both cases, younger middle Miocene sediments were not preserved. This gap is unfortunate because marine and terrestrial proxy data conflict for this time period: evidence for cooling by 15 Ma is based on fossil leaves (Graham, 1999) and the reappearance of cold water minerals in marine sediments in Oregon (Boggs, 1972). In contrast, the marine $\delta^{13}C$ excursion begins at the MMCO at 16 Ma and continues until after 14 Ma (Zachos et al., 2001), suggesting a later onset of cooling.

A well-preserved paleosol at Cricket Flat, near Elgin in eastern Oregon, U.S.A. offers an opportunity to reconstruct paleoenvironment at about 13.8 Ma, during this critical time period. The paleosols best suited for paleoclimate reconstruction (1) are datable; (2) had persisted at the surface long enough to equilibrate with surface conditions; (3) are preserved atop minimally-altered parent material so that chemical alteration is measureable; and (4) are formed on parent material that is sufficiently deep to avoid problems of overprinting from multiple soils formed at similar stratigraphic levels. The Cricket Flat paleosol meets all of these criteria. It is developed on a thick volcaniclastic deposit with minimally altered parent material preserved below the paleosol; it persisted at the surface long enough to develop a strong Bt horizon; and it was buried by an olivine basalt that has been dated, making it ideal for paleoenvironmental reconstruction. In this study, we describe the paleopedology and chemistry of the Cricket Flat paleosol in order to interpret the terrestrial environment at about 13.8 Ma in northeastern Oregon. Supplementary data are available online at http://dx.doi.org/10.1594/PANGAEA.836270.

2. Materials and methods

2.1. Geologic setting

The Columbia River Basalt Group (CRBG) is a large igneous province covering parts of Oregon, Washington, and Idaho (Fig. 1, inset). The largest-volume formations of the CRBG (77.8% of the CRBG; Reidel et al., 2013) are chemically homogeneous basalts and basaltic andesites erupted between about 16 and 15 Ma (Barry et al., 2013 and references therein). As volcanic activity waned after 15 Ma, lava flows became more local and chemically varied. In parts of Washington, northern Oregon and Idaho, the Saddle Mountains Basalt of the CRBG erupted as a sequence of primarily mafic flows beginning with the Umatilla Member at approximately 14.6 Ma (Barry et al., 2013 and references therein). Contemporaneous with the Saddle Mountains Basalt in the southern part of the study area are small-volume alkaline to calc-alkaline lavas and volcaniclastics of the Powder River Volcanic Field (PRVF) and the Oregon–Idaho Graben (Ferns et al., 2010; Ferns and McClaughry, 2013). In some cases paleosols have been preserved between lava flows of the CRBG and PRVF, indicating periods of comparative stability.

Cricket Flat is a small plateau in northeastern Oregon bordered by the Grande Ronde River to the west, the Wallowa Mountains to the south, and by steep ravines cut by the Grande Ronde and Minam rivers to the north and east (Fig. 1). Grande Ronde and Wanapum Basalts from the primary eruptive phase of the CRBG underlie Cricket Flat; a >300 m thick sequence of these flows is visible from the Minam grade of Oregon Route 82, east of the study area. Isolated exposures of volcaniclastic sediments at the base of the PRVF crop out atop Cricket Flat (Fig. 1). These sediments are locally overlain by an approximately 1.5 m thick olivine basalt flow (the Basalt of Little Catherine Creek from the PRVF, Ferns et al., 2010). The volcaniclastic sediments are landslide-prone,

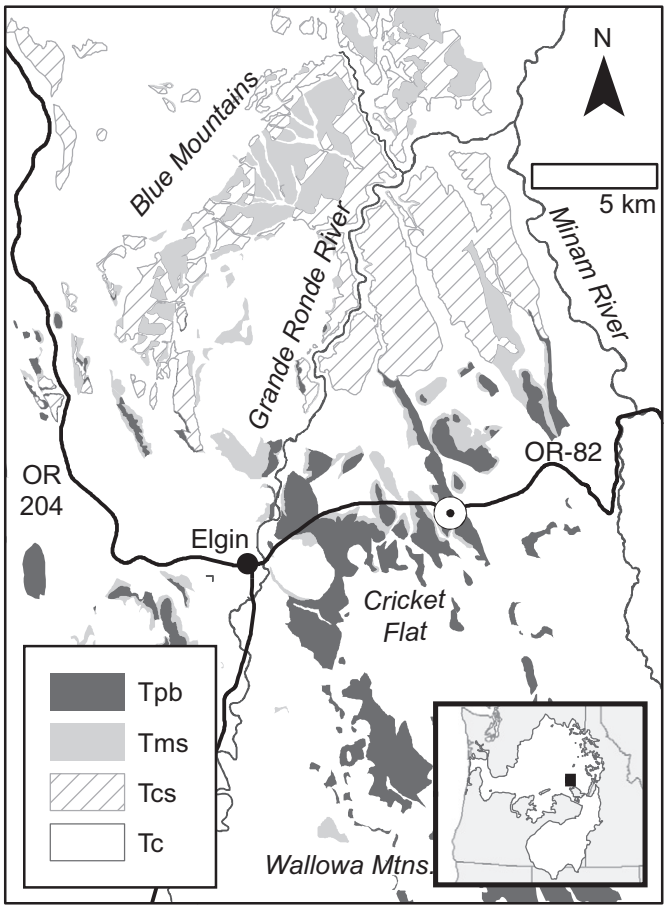

Fig. 1. Inset: study area within the outline of the Columbia River Basalt Group in Washington, Oregon, and parts of Idaho and Nevada, USA (Reidel et al., 2013). Map: Cricket Flat area. Paleosol site is marked as a dot east of Elgin on Oregon Highway 82. Simplified geologic units from Ferns et al. (2010) include Tms (undifferentiated Tertiary sediments including the volcaniclastic parent material), Tpb (the olivine basalt of the Powder River Volcanic Field, Little Catherine Creek member, which overlies the paleosol), and Tcs (Saddle Mountains Basalt, the Columbia River basalt correlative with Tpb). Tc represents undifferentiated basalt flows of the Columbia River Basalt Group. Overlying Quaternary sediments are not shown.

especially when overlain by lava flows (Ferns et al., 2010); consequently they are well exposed only in roadcuts. The Cricket Flat paleosol formed on the volcaniclastic sediments, and was subsequently buried by the eruption of the Basalt of Little Catherine Creek (Figs. 2, 3). The paleosol is readily recognized in the field on the basis of prominent horizons with pale red to pink colors in the uppermost meter (Fig. 2).

Our date estimate for the Cricket Flat paleosol is based on previous work correlated with the overlying olivine basalt. Three $^{40}Ar/^{39}Ar$ dates from Bailey (1990) on the olivine basalt south of the study area are 14.4 ± 0.2 Ma, 13.7 ± 0.1 Ma, and 13.3 ± 0.8 Ma. These dates may come from different flows as there at least 3–4 olivine basalt flows where Bailey's samples were collected, but only a single flow exists at Cricket Flat (the "basalt of Cricket Flat" of Hooper and Swanson, 1990). The olivine basalt at Cricket Flat interfingers to the north with the Umatilla Member of the Saddle Mountains Basalt (Ferns et al., 2010), but the there is only a single K–Ar date from the Umatilla from the U.S. Energy Research and Development Administration (1976). Barry et al. (2013) recalculated the Umatilla Member date to 15.5–12.4 Ma with a most likely date of 14.6 Ma. We calculated the weighted mean of these dates as $\Sigma a_i w_i / \Sigma w_i$, where a_i is age estimate i and w_i is the sample weight, equal to $1 / \sigma^2_i$. To calculate the combined uncertainty, we used the standard deviation of the age estimates, which is more conservative in this case than the weighted error. This calculation puts burial of the Cricket Flat paleosol at ca. 13.8 Ma with a 1-σ uncertainty of 0.6 Ma.

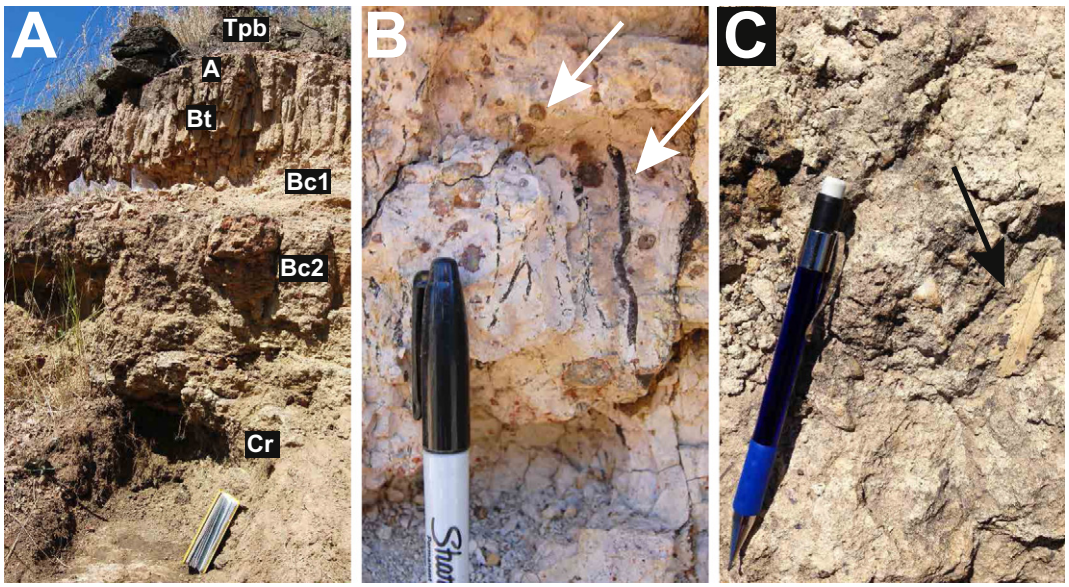

Fig. 2. Field photos of the Cricket Flat paleosol. A: paleosol horizons; note the prominent strong medium prismatic ped structure in the Bt horizon (field notebook is 19 cm tall; see Table 1 for horizon thicknesses). B: root traces and Fe oxide nodules in the A and Ac horizon (black pen cap is 5 cm tall). C: volcaniclastic parent material with leaf fossil, probably *Quercus* sp. (pencil is 14 cm tall).

2.2. Field methods

The site was prepared for description and sampling by excavating visibly weathered or modern material from the surface of the soil profile. Pedogenic features such as horizons and structures were described using standard methods for modern soils (Schoeneberger et al., 2012). Color was measured moist in the field using Munsell soil color charts, and the presence or absence of carbonate was established

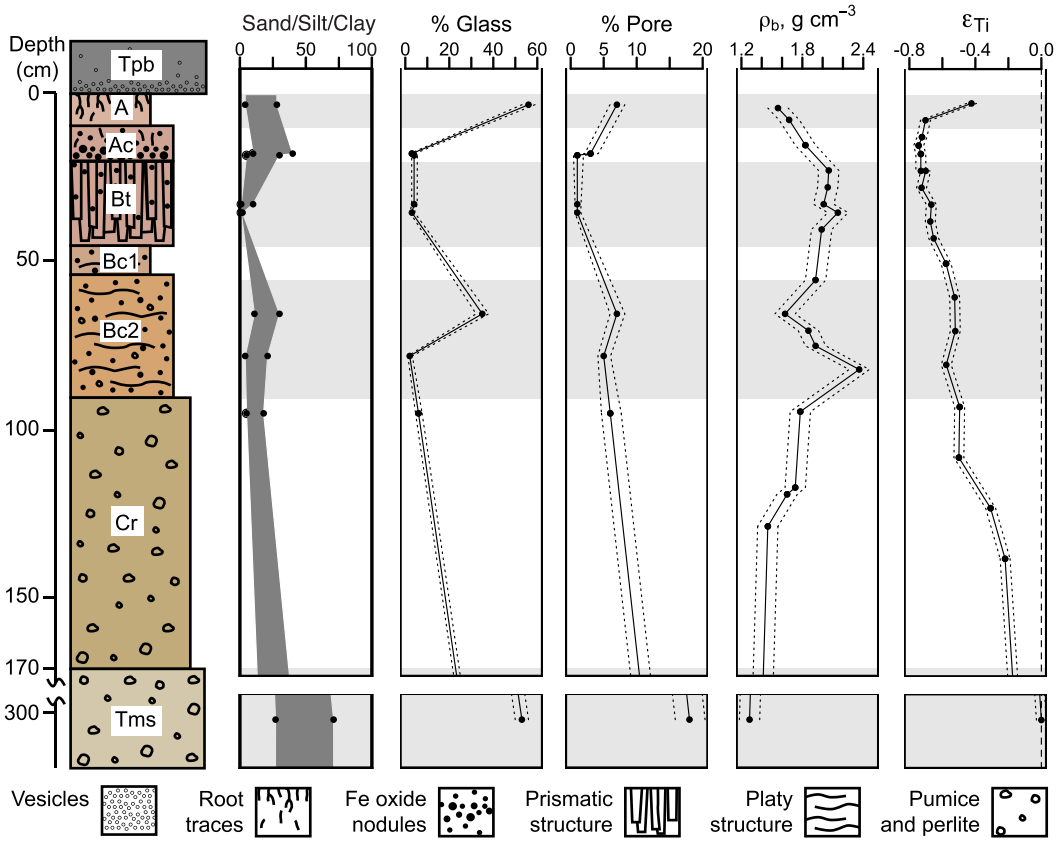

Fig. 3. Generalized stratigraphic section and physical characteristics of the Cricket Flat paleosol. Note break in depth axis between 170 and 300 cm to show comparatively unweathered parent at 305 cm depth. Gray shading in background of plots marks location of soil horizons. ρ_b = bulk density. Dotted lines show 1-σ analytical uncertainty (not shown for texture data); vertical dashed line marks zero point on plot of geochemical strain (ε).

with 5% HCl. Initial assessments of horizon types, horizon boundaries, and pedogenic features were made in the field, and were later confirmed with lab analyses. A suite of 21 samples for geochemical analysis was collected along a depth profile through the paleosol, with samples taken every 5 cm in the top 50 cm of the paleosol and every 10 or more cm below 50 cm depth. Samples were collected in 1-liter poly bags; each sample was at least 250 cm^3 in volume. A second set of 19 oriented, indurated aggregates from different depths was collected for determination of bulk density and for thin sections.

2.3. Bulk chemistry

2.3.1. Sample preparation

The geochemical sample suite was processed and analyzed at the GeoAnalytical Lab in Pullman, Washington, except for initial crushing at Whitman College. The samples were crushed in a jaw crusher with steel plates, then approximately 30 g of chips was hand-picked and ground in a swing mill with tungsten carbide surfaces. Small (3.5 g) subsamples were mixed with di-lithium tetraborate flux and fused at 1000 °C into glass beads that were re-ground, re-fused and polished before analysis on a Thermo-ARL automated X-ray fluorescence spectrometer. This analysis provided the concentration of 10 unnormalized major elements and 19 trace elements for each sample (see online Supplementary data). Two lab replicates run on the same beads yielded indistinguishable values. Based on analysis of a duplicate bead made from the same powder as one of the samples, analytical errors ($\pm 1\sigma$) were less than $\pm 1\%$ for all major elements and less than 1 ppm for all trace elements except for Ba (± 2.1 ppm) and La (± 1.4 ppm). This analytical error was propagated through all calculations to provide estimates of uncertainty.

2.3.2. Identification of immobile element

In order to quantify pedogenic alteration with our geochemical data, we must identify an element that was immobile, i.e., an element that was not added or removed from the parent during pedogenesis. We use the immobile element to define equivalent volumes of parent material and weathered soil. Commonly selected immobile elements include Ti, Zr, and occasionally Al or Nb. We did not consider Nb because of the potential for Nb contamination from the tungsten carbide swing mill (Hickson and Juras, 1986), and we did not consider Al because translocation of aluminosilicate clay minerals is common during pedogenesis. We used the method of Chadwick et al. (1990) to compare the immobility of Ti and Zr, and found both to be similarly immobile. Because Zr is primarily found in zircon crystals in the sand fraction of this paleosol (e.g., Fig. 4), we selected Ti as the least mobile element for more consistent results in our clay-rich soil, as recommended by Stiles et al. (2003).

2.3.3. Geochemical strain

We measured bulk density using the clod method (Blake and Hartge, 1986) on 19 indurated aggregates along a depth profile. Linear interpolation between bulk density measurements provided bulk density at arbitrary depths. We calculated geochemical strain in the weathered soil ($\varepsilon_{Ti,w}$) based on bulk density and concentrations of Ti in the parent and soil, using the method of Brimhall and Dietrich (1987):

$$\varepsilon_{Ti,w} = \frac{\rho_p C_{Ti,p}}{\rho_w C_{Ti,w}}$$

where ρ_p and ρ_w are the bulk density of the parent material and the weathered soil sample, respectively, in units of mass per volume; and $C_{Ti,p}$ and $C_{Ti,w}$ are the concentrations of Ti in the parent and soil, respectively in units of mass per mass.

2.3.4. Geochemical mass balance

Geochemical mass balance (τ) for each element j is calculated from the strain ($\varepsilon_{Ti,w}$) and the concentrations of j in the parent p and the weathered soil w as (Brimhall and Dietrich, 1987):

$$\tau_{j,w} = \frac{\rho_w C_{j,w}}{\rho_p C_{j,p}} \left(\varepsilon_{Ti,w} + 1\right) - 1.$$

This simplifies to:

$$\tau_{j,w} = \frac{C_{j,w} C_{Ti,\,p}}{C_{j,p} C_{Ti,w}} - 1$$

which conveniently makes low-precision bulk density measurements unnecessary for calculating τ.

2.3.5. Provenance and pedogenesis indicators

We assessed homogeneity of the parent material, as well as pedogenic alteration, using ratios of unnormalized major elements. The ratio of Ti to Al, both relatively immobile elements, was used as a provenance indicator (Sheldon and Tabor, 2009). Three bulk chemical indices were used to assess weathering and loss of cations during pedogenesis: (1) the sum of base cations (K, Na, Ca, Mg) divided by Al (Retallack, 1999; Sheldon and Tabor, 2009); (2) the chemical index of alteration minus K (CIA-K; Maynard, 1992), equal to 100 times the ratio Al/(Al + Ca + Na); and (3) the paleosol weathering index for forest soils (PWI = 420 × Na + 166 × Mg + 554 × K + 205 × Ca; Gallagher and Sheldon, 2013). By convention, all of these calculations use moles of major element oxides per unit mass. For example, Ti/Al is calculated as moles of TiO_2 per mole of Al_2O_3. Mean annual temperature (MAT) was calculated from the Bt-horizon average of PWI using Gallagher and Sheldon's (2013) climate transfer function for clay-rich forest soils. Mean annual precipitation (MAP) was calculated from the Bt-horizon average of CIA-K using the function of Sheldon et al. (2002).

2.4. Micromorphology

Ten of the coherent lithified aggregate samples were impregnated with epoxy and cut into oriented thin sections at Spectrum Petrographics in Vancouver, Washington. Thin sections were analyzed using standard petrographic microscope techniques and described according to Stoops (2003). Sand, silt, and clay proportions, and proportions of void space and volcanic glass, were determined by point counting of 300–600 points per thin section. 1-σ uncertainty for point count estimates was calculated using the inverse Beta distribution (Howarth, 1998) with a 2-tailed probability of 84%.

2.5. Clay mineralogy

An approximately 10 cm^3 sample of the Bt horizon was collected for analysis of clay minerals by X-ray diffraction (XRD). The sample was crushed in a jaw crusher, soaked overnight in deionized water, disaggregated wet for 1 min in a blender, and further disaggregated for 5 min with a probe-type sonicator before collecting the <2 μm particle size fraction by centrifugation.

Subsamples were saturated with either 0.1 M MgCl or 1 M KCl and transferred to glass slides using the filter transfer method of Drever (1973) to obtain oriented samples. Three treatments were used: (1) Mg-saturated and air-dried; (2) Mg-saturated and fumigated with ethylene glycol; and (3) K-saturated and heated to 550 °C for 3 h in a muffle furnace before analysis. The oriented samples were analyzed in a Siemens D-500 X-ray diffractometer at Washington State University with CuKα radiation and a range of 2–32°2θ, a step size of 0.05°2θ, and a count time of 10 s. Clay minerals were identified using standard techniques outlined in Moore and Reynolds (1997).

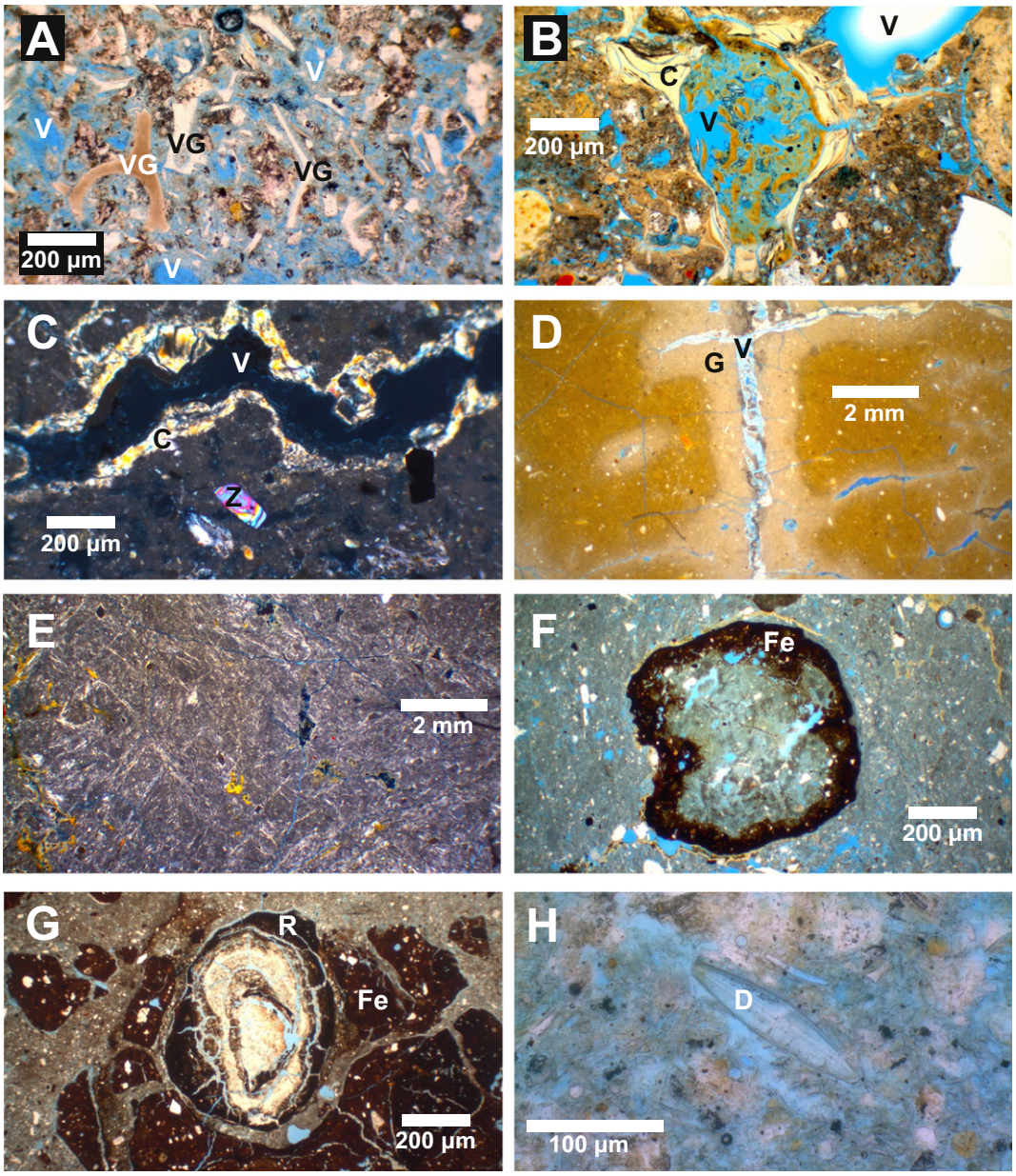

Fig. 4. Photomicrographs of the Cricket Flat paleosol, in plane polarized (PPL) and cross polarized light (XPL), arranged by decreasing depth beneath the paleo-surface. Up orientation is towards the top of the page; blue areas are stained epoxy filling void space. A: (PPL) abundant volcanic glass (VG) fragments and voids (V) in parent material, 12 m depth; B: (PPL) illuvial clay coatings (C) in a void (V), Cr horizon, 95 cm depth; C: (XPL) birefringent illuvial clay coatings (C) around void (V) and zircon crystal Z, Bc2 horizon, 78 cm depth; D: (PPL) gleyed haloes (G) around voids (V), Bt horizon, 35 cm depth; E: (XPL) cross-striated b-fabric in crossed polars, Bt horizon, 32 cm depth; F: (PPL) Fe oxide nodule, Ac horizon, 18 cm depth; G: (PPL) root trace (R) and Fe oxide nodules, Ac horizon, 17 cm depth; H: (PPL) diatom (D) and phytoliths, A horizon, 3 cm depth.

3. Results

3.1. Parent material (below 170 cm depth)

The paleosol is developed on the upper 170 cm of a volcaniclastic deposit described as a rhyolitic lithic tuff by Carson (2001) and Ferns et al. (2010). Ferns et al. (2010) mapped this material as Tms, undifferentiated Tertiary sediments and noted that this unit reaches thicknesses of 150 m in a drill core obtained approximately 10 km to the northwest. This white volcaniclastic deposit contains oak-like leaf imprints and charred wood fragments (Fig. 2). White, rounded to subrounded pumice clasts up to about 4 cm are abundant; adjacent obsidian fragments are generally smaller (typically less than 1 cm) and angular to subangular. Angular to subrounded lithic clasts, mostly from silicic volcanic rocks, comprise approximately 2–5% of the unit by volume. The largest lithic clasts are up to 30 cm diameter but most are ~2–4 cm diameter. Perlite spherules are also present. There is at least one apparent log mold filled with silt and clay exposed in the road cut at Cricket Flat. No parent materials show preferred orientation.

Based on point counts from two thin sections obtained at 1215 cm and 305 cm depth below the upper contact (Fig. 4A), approximately 15% of the deposit is macropore space, and the bulk density is consequently low, ~1.3 g cm^{-3}. The solid non-clay-size fraction is about 75% glass, 15% crystals, and 10% lithic fragments. The lithic fragments consist typically of flow-banded rhyolite and obsidian that is remarkably angular. Both fragile bicuspate and tricuspate glass shards (<1 mm) and pumice comprise the vitric fraction. In thin section, pumice clasts are not obviously abraded and may appear rounded in outcrop because of partial weathering to clay and disaggregation. The crystalline component includes fine to medium grained plagioclase grains, many

exhibiting deformation twinning and internal zoning. Nearly all of these phenocrysts are broken with grain edges crossing internal compositional zoning. There are a few glomeroclots of plagioclase and plagioclase + K feldspar. Small crystals of K feldspar and magmatic epidote are both present, as well as apatite, zircon, and hematite. Quartz is present though much less abundant than plagioclase. Occasional isolated fragments of clay aggregates not associated with fractures or pores are visible in thin section. One thin section taken from 65 cm below the top contact is remarkable for a greater abundance of pumice (Fig. 3).

3.2. Cr horizon (170 to 90 cm depth)

The lower boundary of the Cr horizon is diffuse, occurring at approximately 170 cm below the contact with the olivine basalt. In outcrop, the Cr horizon looks similar to the underlying parent material except for a pale brown color and greater concentration of small fractures. In thin section, however, the Cr and R horizons are very distinct (Fig. 4A–B). Point counts reveal that the Cr horizon contains dramatically of the clay-sized fraction than the parent (82% vs 26–29%, respectively), and less glass in the silt to sand sized fraction (Fig. 3). Much of the additional clay-size fraction is in the form of fine-grained matrix, but oriented domains of clay coat macropore walls (Fig. 4B).

3.3. B horizon (90 to 20 cm)

The boundary between the C and B horizons is a gradual transition around 90 cm depth. The B-horizon lacks carbonate throughout, as does the parent material and the remainder of the soil profile. Root traces are not apparent in the field and are rare in thin section. The B horizon consists of a lower reddish-yellow Bc horizon 45 cm thick (note that the "c" subscript refers to nodules or concretions, not to the C horizon) with platy structure and common light red Fe nodules, overlain by a strongly prismatic pale red Bt horizon 25 cm thick with fewer and smaller red Fe nodules (Figs. 2, 3, Table 1). A sample of the horizon at about 65 cm is locally enriched to about 35% primary volcanic glass weathering to clay (Figs. 2, 3), primarily due to abundant coarse pumice clasts in this sample. From point counts, the Bt horizon has very high clay content, between 90 and 99% clay-sized particles (Figs. 3, 4D, E). Under crossed polars in thin section, the Bt horizon clay is aligned in birefringent domains, giving it a characteristic cross-striated b-fabric and near-vertic appearance (Fig. 4E). In outcrop the ped interiors often appear darker; this is also visible in thin section as gleying along fractures (Fig. 4D). The Bt horizon appears to have been a seasonally-impermeable barrier based on its high clay content and on the rarity of root traces in the field below the A horizon.

From XRD analysis, the dominant clay mineral in the <2 μm fraction of the Bt horizon is smectite, based on the expansion of the 14–14.5 Å peak to near 16 Å with glycol solvation and the collapse of the 14.5 Å peak with K-saturation and heating to 550 °C (Fig. 5). The 14.5 Å peak does not persist with glycolation or heating, ruling out vermiculite and chlorite. Minor amounts of kaolinite and illite may be present, due to small peaks for kaolinite at 3.5 and 7 Å and illite near 10 Å. Quartz peaks are visible in all treatments at around 3.3 and 4.2 Å. The 4.2 Å peak has a broad shoulder on the right (Fig. 5) that is characteristic of opaline silica diagenetically transforming to crystalline quartz (Moore and Reynolds, 1997).

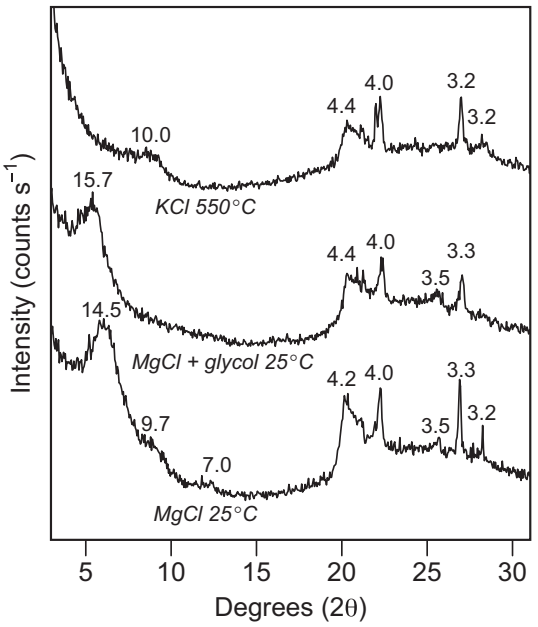

Fig. 5. X-ray diffraction patterns of the <2 μm equivalent particle size fraction from the Bt horizon of the Cricket Flat paleosol. Numbers above peaks are measured d-spacings. See text for interpretation of peaks.

3.4. A horizon (20 to 0 cm)

The transition from the B to A horizon at 20 cm depth is abrupt and wavy. A pale red indurated Ac horizon about 10 cm thick, containing common medium to coarse prominent red Fe nodules (Figs. 2, 4F, G), is overlain by a more friable pale A horizon with rare nodules but common mineralized root traces. The A horizon is comparatively rich not only in sand and silt-sized primary glass fragments but also in biogenic siliceous material, with occasional phytoliths and soil-dwelling diatoms (Fig. 4H). A meter-wide zone of this horizon and the Bt horizon is uniformly gleyed in outcrop and in thin section (Fig. 4F).

3.5. Bulk chemistry

Chemical variations through the soil profile are shown in Fig. 6. The Ti/Al indicator of parent material provenance is homogeneous throughout the profile except for a positive excursion in the Ac horizon due to reduced Al. Depth profiles of geochemical mass balance are dominated by depletion of major elements relative to Ti ($\tau < 0$, Fig. 6). The

Table 1
Horizon descriptions for the Cricket Flat paleosol. Depths are below the upper contact with the olivine basalt; standard terms for lower boundary and structure are as defined in Schoeneberger et al. (2012).

Depth (cm)	Horizon	Dry Munsell color	Lower boundary	Structure
0 to 10	A	2.5 YR 8/3 to 7/4, pink to light reddish brown	Gradual, smooth	Moderate medium angular blocky
10 to 20	Ac	10 R 7/4, pale red	Abrupt, wavy	Strong coarse angular blocky
20 to 45	Bt	10 R 7/3, pale red	Clear, wavy	Strong medium prismatic
45 to 55	Bc1	5 YR 7/4 pink	Smooth, gradual	Moderate medium platy
55 to 90	Bc2	7.5 YR 7/6, reddish yellow	Smooth, gradual	Strong medium to thick platy
90 to 170	Cr	2.5 Y 7/4, pale brown	Diffuse	Massive, fractured
>170	R	2.5 Y 8/1 to 8/2, white to pale brown	–	Massive

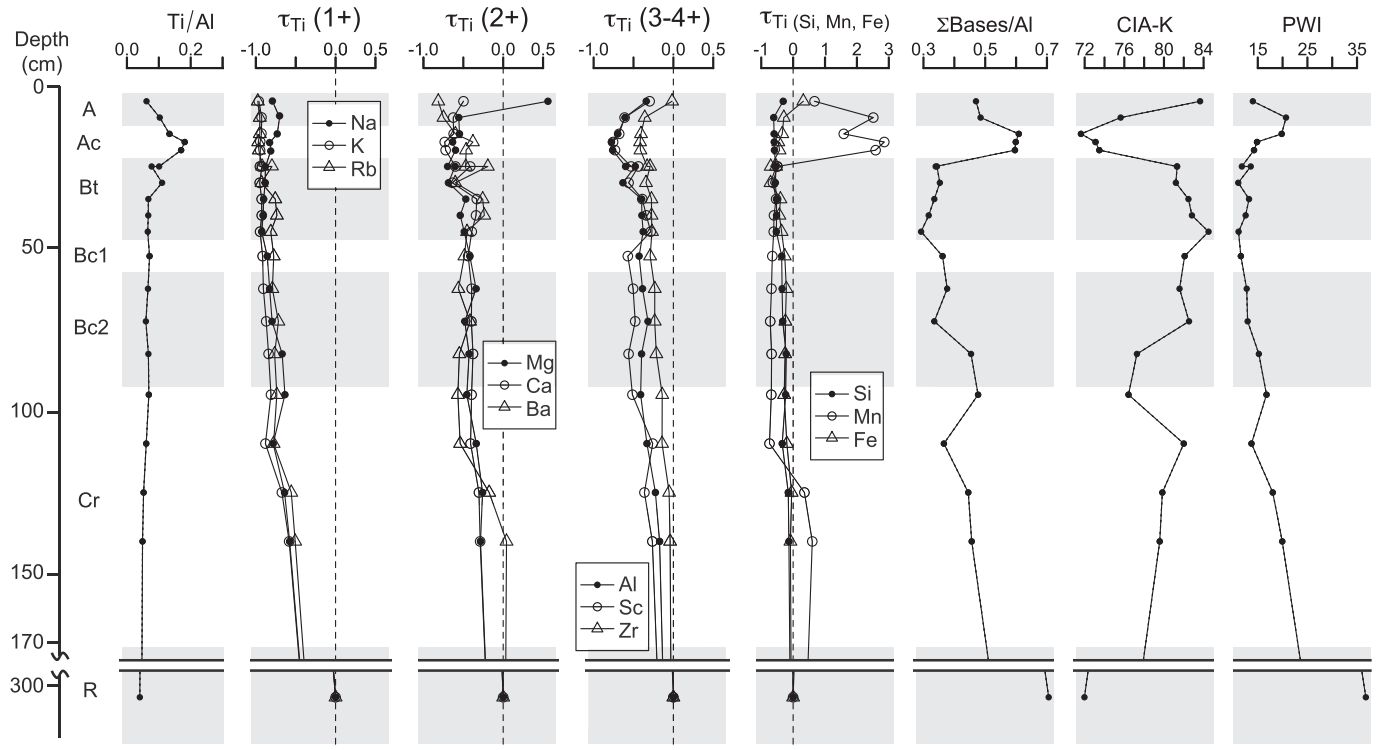

Fig. 6. Bulk chemical indicators of weathering along depth profiles in the Cricket Flat paleosol. Note break in depth axis is the same as Fig. 3; gray shading on plots marks location of soil horizons. Ti/Al is a provenance indicator. τ_{Ti} plots are depth profiles of geochemical mass balance of major and trace elements relative to Ti; parent composition is shown by the dashed vertical line at $\tau = 0$. Element depletion ($\tau < 0$) is common. ∑Bases/Al, CIA-K, and PWI are geochemical indicators of weathering; weathering increases to the right for CIA-K and to the left for ∑Bases/Al and PWI. 1-σ analytical error is smaller than the symbol size for all plots.

monovalent cations Na, K and Rb, which are particularly susceptible to weathering and subsequent leaching, have been almost completely depleted from the upper part of the soil profile (complete loss relative to Ti is $\tau = -1$). The divalent cations Mg, Ca, and Ba have similar depletion profiles but are not as depleted relative to equivalent volumes of parent material (Fig. 6). Relatively less of the trivalent (Al and Sc) and tetravalent (Zr) cations was lost from the soil. However, depletion of these relatively immobile elements is nonetheless evident, especially from the Ac horizon (Fig. 6).

The weathering indicators (∑Bases/Al, CIA-K, and PWI) all plot in a similar pattern with the values indicating the most weathering in the B horizon (Fig. 6, Table 2). The ∑Bases/Al and CIA-K indicators apparently indicate less intense weathering in the Ac horizon but mass balance calculations show that this excursion is driven by additional Al loss in the lower A horizon, not by reduced cation loss (Fig. 6).

Despite significantly higher abundance of Fe nodules in the Ac and Bc horizons, the Fe profile is uniformly depleted. This indicates that Fe nodules represent local redistribution of Fe rather than zones of Fe accumulation. Mn, in contrast, is dramatically higher in the A and Ac horizons (Fig. 6). In the field, Mn oxides coat some ped surfaces in the A horizon, and Mn oxides are also concentrated around root traces (Fig. 2). Si is depleted throughout the profile and no zones of Si redeposition are evident (Fig. 6).

Table 2
Indices of chemical weathering (mean ± σ), calculated for the minimally weathered parent material and the mean of the Bt horizon: ∑Bases/Al (Retallack, 1999; Sheldon and Tabor, 2009); the chemical index of alteration minus K (CIA-K; Maynard, 1992), and the paleosol weathering index for forest soils (PWI; Gallagher and Sheldon, 2013).

Index	Parent	Bt mean
∑Bases/Al	0.706 ± 0.003	0.330 ± 0.022
CIA − K	72.0 ± 0.1	82.3 ± 1.3
PWI	36.8 ± 0.1	12.2 ± 1.1

4. Discussion

4.1. Nature of the volcaniclastic parent

The volcaniclastic unit on Cricket Flat has been called a silicic ash-flow tuff (Hooper and Swanson, 1990; Carson, 2001) and a rhyolitic lithic tuff (Ferns et al., 2010), indicating that the unit was deposited as a pyroclastic flow. Carson (2001) suggested that it may alternatively have been a lower temperature debris flow or lahar deposit. The presence of preserved leaf fossils and a tree mold supports the latter hypothesis, though the charred wood fragments found by us and by Carson (2001) are somewhat contradictory. We did not comprehensively sample and describe the internal stratigraphy below the top 3 m, though isolated clay aggregate inclusions seen in thin section suggest that the tuff was reworked. If so, transport distances were relatively short, and water content of the debris flow was not sufficient to create any bedding features or sort clasts by size and density. Moreover, mm-to-cm-scale lithic fragments and broken phenocrysts are notably angular and fragile glass shards are intact in that none show rounding or adjacent broken fragments. Glass content is locally heterogeneous in the parent material (Fig. 3) and the increased abundance of silt-to-sand-sized glass in the A horizon could be consistent with a co-ignimbrite ash. Whether this rhyolitic ash-flow tuff is reworked or not, it is remarkably chemically homogeneous above and below the Ac horizon (Ti/Al = 0.08 ± 0.04 overall, Fig. 6). This variability in Ti/Al is well within the range expected for a soil developed on a single parent material (soils developed on mudstone and basalt reported in Sheldon and Tabor, 2009). In addition, uniform depth profiles of cation loss (Fig. 6) indicate that a single paleosol developed on a single parent material.

4.2. Pedogenic vs non-pedogenic properties

Before interpreting pedogenic processes, we attempt to distinguish between paleosol properties resulting from pedogenic and non-

pedogenic processes. For example, the excursion in Ti/Al in the Ac horizon (Fig. 6) could result from primary heterogeneity in the volcaniclastic deposit (e.g., two-stage deposition with the uppermost 20 cm deposited in a separate event). Alternatively, preferential loss of Al relative to Ti could have been pedogenic (leaching and the eluviation of aluminosilicate clays from the Ac horizon) or diagenetic (leached by reduced groundwaters following burial). However, two-stage deposition of the parent is unlikely because the excursion in Ti/Al is comparatively small and the uppermost samples in the A horizon are identical in Ti/Al to the parent material. Also, while diagenetic loss of Al may have occurred, pedogenic loss is plausible because the fluctuating redox conditions indicated by the iron nodules in the Ac horizon (Zhang and Karathanasis, 1997) would have allowed Al to be redistributed.

Thermal diagenesis is another important potentially confounding factor affecting paleosol properties. Certainly, the eruption of the olivine basalt heated the soil. Although the olivine basalt and the Ac horizon have reversed magnetic polarity, the deeper parent material lacks a significant paleomagnetic signature (R. Rodd and K. Verosub, personal communication), suggesting that the basalt flow heated the A horizon significantly. However, there is no strong evidence that the heating was pervasive at depth or altered the micromorphology of the soil. This is supported by other studies that report minimal physical and chemical alteration at depths greater than 10 cm beneath lava flows in various types of paleosols including histic paleosols on basalt (Sheldon, 2003), Terra Rossa-type paleosols developed on chalk (Smith and McAlister, 1995), and paleosols developed on granites in the Auvergne (Pierre, 1990; cited in Smith and McAlister, 1995). Carson (2001) suggested that the reddened color and vertical prisms of the Cricket Flat paleosol could have resulted from thermal alteration from the overlying olivine basalt flow. Paleosols can become redder after burial by growth of hematite crystals (Blodgett, 1988) or dehydration of iron hydroxides to hematite (Retallack, 1991). However, the vertical prisms in the Bt horizon have a distinctive cross-striated b-fabric in thin section, indicating a pedogenic origin.

The most significant non-pedogenic chemical alteration in this paleosol was probably the oxidation and loss of soil organic matter. There is virtually no visible organic matter remaining in the paleosol, consistent with the typical results of post-burial decomposition (e.g., Kraus, 1999). Locally there is meter-scale gleying of the Bt horizon apparent in outcrop. In thin sections from oxidized areas of the Bt horizon, this gleying is restricted to the area around void spaces representing the most recent joints in the Bt horizon (Fig. 4D), suggesting that it was a result of chemical reduction of iron following burial of the paleosol (Retallack, 1991). This probably had a minor effect on our analysis, as Bt horizon samples from oxidized and gleyed regions are not significantly different in their bulk chemistry.

Post-burial compaction can significantly affect some buried paleosols, but compaction of the Cricket Flat paleosol was probably minimal. This paleosol was probably never deeply buried since the overlying basalt is only about 4 m thick; even if the original thickness of the basalt was 30 m (the approximate maximum olivine basalt flow thickness measured from well logs near Imbler to the south, reported in Ferns et al., 2010) compaction of this paleosol was negligible, based on Sheldon and Retallack's (2001) equation. Furthermore, the parent has high macroporosity at 3 m depth (Figs. 3, 4A).

4.3. Paleosol classification

Although modern soils can be unequivocally classified, paleosol classification is somewhat subjective. The Cricket Flat paleosol is an Argillisol in the Mack et al. (1993) classification scheme, based on the prominent Bt horizon and the lack of pedogenic carbonate. Although the paleosol has distinctly vertic features in thin section (Fig. 4E) and abundant smectite (Fig. 5), these features are not unique to Vertisols (Nettleton and Sleeman, 1985), and the clearly defined horizons and the lack of slickensides or wedge-shaped aggregates rules out a Vertisol in either the Mack or USDA soil classification system (Soil Survey Staff, 2014). The Argillisol taxon includes both USDA Alfisol and Ultisol soil orders (Mack et al., 1993). Modern Alfisols and Ultisols are distinguished on the basis of cation exchange capacity (CEC), in that Alfisols are defined by a CEC of at least 35% and Ultisols are defined by CEC <35% (Soil Survey Staff, 2014). Because the Cricket Flat paleosol is indurated, we cannot be confident that measurements of CEC would be faithful to the original soil chemistry. However, Sheldon et al. (2002) found that the ratio of summed bases (Ca + Mg + Na + K) divided by Al in the B-horizon is a statistically significant proxy for CEC in modern soils, with values less than 0.5 equivalent to Ultisols. The Cricket Flat paleosol has low $\sum$Bases/Al throughout, with the lowest values of 0.33 ± 0.02 in the Bt horizon (Fig. 6). Furthermore, the highly depleted τ profiles for elements such as K and Na (Fig. 6) are consistent with a deeply-weathered Ultisol. Weathering of silicate rocks results in a net consumption of atmospheric CO_2 (Berner et al., 1983). Based on Sheldon and Tabor's (2013) calculation using the total calculated loss of base cations, deep pedogenic weathering of the Cricket Flat paleosol consumed a total of about 0.35 mol CO_2 cm^{-2} (about 160 kg CO_2 m^{-2}). This is slightly less than the Alfisols in the Picture Gorge Basalts because of the low base status of the unweathered parent material.

4.4. Paleoenvironment implications

An Ultisol-like paleosol of Miocene age in eastern Oregon is surprising. In eastern Oregon and Washington, highly weathered Ultisol-like paleosols are known from the Eocene (e.g., Bestland et al., 1996) but not thereafter (Retallack, 2009a). To our knowledge, no other Ultisol-like soils from the Neogene to the present have been identified from eastern Oregon. Modern Ultisols in Oregon exist only in a narrow, rainy region near the coast; east of the Cascade Mountains, a significant rain shadow prohibits the development of Ultisols (MAP < 300 mm $year^{-1}$ east of the Cascades, compared to 1500–2000 mm $year^{-1}$ west of the Cascades; Kohn et al., 2002). Thus, the Cascade rain shadow may have been weaker during the formation of the Cricket Flat paleosol. The Cascade rain shadow was probably at least partly developed in Oregon by the late Eocene (Sheldon et al., 2002; Sheldon and Retallack, 2004), long before the Cricket Flat paleosol. However, there is evidence that the rain shadow was weaker in the Miocene: Takeuchi and Larson (2005) found that significant strengthening of the rain shadow effect in southern Washington, equivalent to ~1.2–1.7 km of Cascades uplift, has occurred only during the last 15.6 Ma.

Our ability to judge the broader paleoenvironmental context of this paleosol is partly limited by the lack of other exposed paleosols from the same stratigraphic position. The unusually extensive weathering we observe in this paleosol is probably partly due to glass-rich parent material; the glass fraction of the parent is susceptible to weathering, so less weathering is necessary to generate an Ultisol on this parent material than on other parent compositions. Thus, in the middle Miocene landscape, Ultisols may have coexisted with Alfisols on different parent materials. In the Piedmont region of the southeastern United States, predominantly Ultisols on felsic parent of granite, gneiss, and schist coexist with Alfisols developed on gabbro and diorite (Rice et al., 1985; Shaw et al., 2001), probably due to the higher base status of mafic rocks. Similarly, Ultisols and Alfisols coexist today in Oregon west of the Cascade Mountains (Parsons, 1978).

Modern Ultisols form in areas of landscape stability, although they occasionally form in as little as 12 thousand years (Gamble et al., 1970). Using Sheldon's (2003) formula for the time of formation based on the thickness of the Bt horizon [$T = 17.07B^2 + 645.8B$, where T is formation duration (y) and B is the thickness of the Bt horizon (cm)], we estimate that the soil formed over a period of at least 27 ky prior to the eruption of the olivine basalt. However, this estimate may be too low because the clay-rich Bt horizon probably formed a seasonal barrier to infiltrating water that slowed clay eluviation. The age of the volcaniclastic parent is unknown, but it may be related to other

rhyolitic deposits further to the south, tentatively dated between 15.5 and 14.7 Ma (Ferns and McClaughry, 2013); this is an upper limit on the time available for pedogenesis.

Based on Gallagher and Sheldon's (2013) relationship between Bt horizon PWI (Fig. 6) and MAT for forest-type soils, we calculate a MAT of 14.5 ± 2.1 °C for the Cricket Flat paleosol. MAP calculated using the CIA-K proxy (Sheldon et al., 2002) is 1120 ± 180 mm year^{-1}. Based on modern mean temperature and precipitation data (1981–2010 means; PRISM Climate Group, 2012) and modern soils data (the STATSGO2 dataset; Soil Survey Staff, 2003), the nearest Ultisols currently forming in this general range of conditions are Humults that occur locally in the coast ranges of southwestern Oregon and northwestern California. However, these soils tend to experience cooler and wetter conditions than we calculate for the Cricket Flat paleosol. Better modern analogs for the Cricket Flat paleosol are Xerults found along the western flanks of the Sierra Nevada Mountains in northern California between about 500 and 1000 m elevation, including the Jocal and Sites series soils. In the eastern United States, Ultisols in this range of temperature and rainfall conditions are most common in the Piedmont region, especially in North Carolina and Virginia.

4.5. Correlation with other paleoenvironment records

Our understanding of middle Miocene climate comes from a variety of proxy datasets, not all of which agree. Perhaps the most continuous record comes from calcareous nanofossils in marine sediments. Zachos et al. (2001) compiled a global $\delta^{18}O$ and $\delta^{13}C$ dataset using marine nanofossils from more than 40 cores worldwide. The period from about 17–14 Ma is marked by a broad minimum in mean $\delta^{18}O$, which is usually interpreted as representing warmer deep ocean water and smaller polar ice caps associated with the MMCO (e.g., Holbourn et al., 2007). This is in general agreement with our findings, which indicates warm and wet conditions around 14 Ma (Fig. 7).

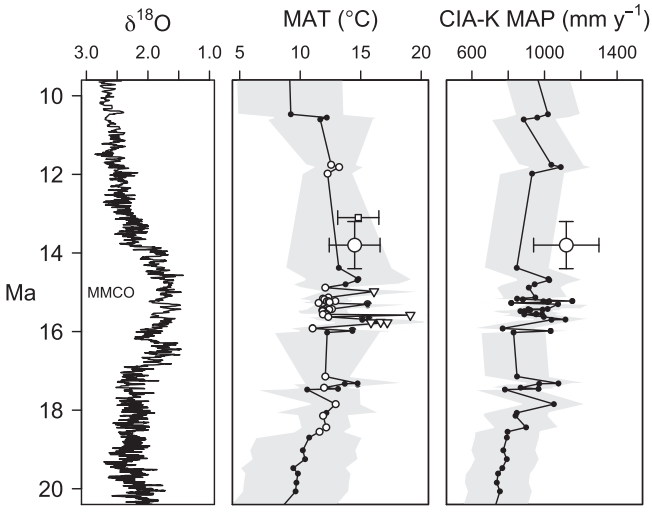

Fig. 7. Miocene marine and terrestrial climate proxies, 20–10 Ma. Left: marine $\delta^{18}O$ record from benthic foraminifera, "MMCO" marks the middle Miocene climatic optimum. Middle: mean annual temperatures calculated from paleosols of Oregon and Washington. Black circles: MAT from Oregon paleosols of the Retallack (2007) dataset using the salinization proxy (Sheldon et al., 2002). Open circles: forest-type paleosols from the same dataset recalculated using the PWI proxy of Gallagher and Sheldon (2013). Triangles: Washington paleosols from Takeuchi et al. (2007), using the salinization proxy. Shaded area is the standard error of the MAT proxy (±4.4 °C for salinization MAT; ±2.1 °C for PWI MAT). Large open circle is PWI-derived MAT from the Cricket Flat paleosol, this study; white square is a CLAMP-based temperature estimate from a leaf assemblage in Oregon (Wolfe et al., 1997). Right: mean annual precipitation calculated using the CIA-K relationship of Sheldon et al. (2002) for all Oregon paleosols from Retallack (2007). Shaded area is ±181 mm year^{-1}, the standard error of the CIA-K–MAP regression relationship. Large open circle is the MAP estimate from the Cricket Flat paleosol, this study. Vertical error bars on the Cricket Flat paleosol are from the age uncertainty of the overlying basalt.

Although the marine data are useful for characterizing global averages in climate, terrestrial proxies are more useful for understanding local-scale paleoenvironments. However, terrestrial records have lower temporal resolution, so they are more challenging to correlate. Most terrestrial records reveal a warm MMCO centered at about 16 Ma, but they differ in the timing of post-MMCO cooling. MAP and MAT estimates from the Cricket Flat paleosol are consistent with paleosols developed during the MMCO (Fig. 7) suggesting that the return to cooler and dryer conditions was not complete by 15 Ma in this region. The paleosol record from Oregon (Retallack, 2007) and eastern Washington (Takeuchi et al., 2007) reveals episodic warm and rainy conditions between 16 and 15 Ma, possibly followed by cooler and dryer conditions between 15 and 14 Ma: the handful of paleosols dating from just after 15 Ma are similar in weathering and salinization to paleosols from before 16 Ma (Fig. 7). However, the interval between 15 and 12 Ma is notably sparse in the Oregon and Washington paleosol record, and there is ample room for interpretation. Other paleosol records from different parts of the world are also missing this time period. For example, the Nebraska paleosols described in Retallack (2007) are sparse during the same period as the Oregon paleosols, and the south Australian record from Lake Palankarinna lacks paleosols between 15 and 10 Ma (Metzger and Retallack, 2010). Paleosol records with data during this interval differ in their details. For example, Kenyan paleosols of the middle Miocene Maboko Formation indicate a return to dry conditions by 15 Ma, with a slight rebound to warmer and wetter conditions by 14 Ma (Retallack et al., 2002). The paleosols from Railroad Canyon in Idaho and Montana show a similar precipitation pattern but do not capture a temperature increase during the MMCO (Retallack, 2009b). Although the Cricket Flat paleosol is a single data point in this record, it suggests that post-MMCO cooling was not complete by about 13.8 Ma.

Terrestrial fossil assemblages also enable reconstruction of local paleoclimate, so they should ideally support an interpretation that is consistent with other climate proxies. The late onset of post-MMCO cooling suggested by the Cricket Flat paleosol is consistent with MAT estimates of 14.8 °C from the 13.1 Ma Molalla plant assemblage near Portland, Oregon, using the CLAMP proxy (Wolfe et al., 1997). Terrestrial vertebrate faunal assemblages are more difficult to correlate. In the fossil record of North American land mammals, such as that at Railroad Canyon, the Barstovian stage contains the period between about 16 and 14 Ma critical for interpretation of the Cricket Flat paleosol. There is a significant species-richness peak in land mammal fossils during the early part of the Barstovian in the northwestern United States, followed by a reduction in species richness by the early Late Barstovian (Barnosky and Carrasco, 2002), at about the time of the Cricket Flat paleosol. However, Barnosky and Carrasco (2002) cautioned that there is no strong link between global temperature change and species richness through time. In any case, using mammal changes to correlate between climate records is somewhat problematic because many mammal localities, like the Railroad Canyon sequence, are partly dated using biostratigraphy (Barnosky et al., 2007). Clearly, there are unresolved differences among terrestrial paleoclimate proxies, due to the importance of regional variability in terrestrial environments. Discovery and analysis of more paleosols from this time and region would greatly help to disentangle landscape-level factors, such as topography, from regional-level climate influences.

4.6. Conclusions

The Cricket Flat paleosol is a remarkably well-preserved Ultisol-like paleosol from 13.8 ± 0.6 Ma in eastern Oregon. Analysis of bulk chemistry shows that the soil was deeply weathered relative to the volcaniclastic parent material. Temperature and moisture indicators suggest that northeastern Oregon was still warm (MAT 14.5 ± 2.1 °C) and wet (MAP 1120 ± 180 mm year^{-1}) during this time despite post-middle Miocene climatic optimum cooling between 16 and 13.9 Ma.

Acknowledgments

This project was funded by the Keck Geology Consortium member institutions, the National Science Foundation (NSF-REU Grant 1062720), and the ExxonMobil Corporation. Mark Ferns and Jason McClaughry (Oregon Department of Geology and Mineral Industries), Jay Van Tassell (Eastern Oregon University), R. "Bud" Wobus (Williams College) and Patrick Spencer (Whitman College) visited our field site and provided their insight and advice. Greg Retallack (Oregon State University) kindly provided field notes from his earlier site visit. Rick Conrey (Washington State University, Pullman) at the GeoAnalytical lab provided student training and XRF analyses. Rebecca Rodd (UNC Chapel Hill), Dennis Geist (U of Idaho), Meagen Pollock (College of Wooster), and Ken Verosub (UC Davis) assisted the authors with their analyses following the field season. Jim and Holly Akenson kindly made their land available to our group during the field season. We thank Nathan Sheldon, an anonymous reviewer, and the Editor, who made helpful comments on an earlier draft that significantly improved the quality of this article.

Appendix A. Supplementary data

Supplementary data associated with this article can be found in the online version, at http://dx.doi.org/10.1016/j.geoderma.2014.10.007. These data include a Google map of the study area.

References

Bailey, D.G., 1990. Geochemistry and Petrogenesis of Miocene Volcanic Rocks in the Powder River Volcanic Field, Northeastern Oregon(Dissertation) Washington State University, Pullman, Washington.

Barnosky, A.D., Carrasco, M.A., 2002. Effects of Oligo-Miocene global climate changes on mammalian species richness in the northwestern quarter of the USA. Evol. Ecol. Res. 4, 811–841.

Barnosky, A.D., Bibi, F., Hopkins, S.S., Nichols, R., 2007. Biostratigraphy and magnetostratigraphy of the mid-Miocene Railroad Canyon Sequence, Montana and Idaho, and age of the mid-Tertiary unconformity west of the continental divide. J. Vertebr. Paleontol. 27, 204–224.

Barry, T.L., Kelley, S.P., Reidel, S.P., Camp, V.E., Self, S., Jarboe, N.A., Duncan, R.A., Renne, P.R., 2013. Eruption chronology of the Columbia River Basalt Group. In: Reidel, S.P., Camp, V.E., Ross, M.E., Wolff, J.A., Martin, B.S., Tolan, T.L., Wells, R.E. (Eds.), The Columbia River flood basalt province. Geological Society of America Special Paper 497, pp. 45–66.

Berner, R.A., Lasaga, A.C., Garrels, R.M., 1983. The carbonate–silicate geochemical cycle and its effect on atmospheric carbon dioxide over the past 100 million years. Am. J. Sci. 283, 641–683.

Bestland, E.A., Retallack, G.J., Rice, A.E., Mindszenty, A., 1996. Late Eocene detrital laterites in central Oregon: mass balance geochemistry, depositional setting, and landscape evolution. Geol. Soc. Am. Bull. 108, 285–302.

Bestland, E.A., Forbes, M.S., Krull, E.S., Retallack, G.J., Fremd, T., 2008. Stratigraphy, paleopedology and geochemistry of the middle Miocene Mascall Formation (type area, central Oregon, USA). PaleoBios 28, 41–61.

Blake, G.R., Hartge, K.H., 1986. Bulk density. In: Klute, A. (Ed.), Methods of Soil Analysis Part I — Physical and Mineralogical Methods. Soil Science Society of America, Madison, Wisconsin, pp. 363–382.

Blodgett, R.H., 1988. Calcareous paleosols in the Triassic Dolores Formation, southwestern Colorado. In: Reinhardt, J. (Ed.), Paleosols and Weathering Through Geologic Time: Principles and Applications. Geological Society of America, Boulder, Colorado, pp. 103–121.

Boggs, S., 1972. Petrography and geochemistry of rhombic, calcite pseudomorphs from the mid-Tertiary mudstones of the Pacific Northwest, U.S.A. Sedimentology 19, 219–235.

Brimhall, G.H., Dietrich, W.E., 1987. Constitutive mass balance relations between chemical composition, volume, density, porosity, and strain in metasomatic hydrochemical systems: results on weathering and pedogenesis. Geochim. Cosmochim. Acta 51, 567–587.

Carson, R.J., 2001. Where the Rockies meet the Columbia Plateau: geologic field trip from the Walla Walla Valley to the Wallowa Mountains, Oregon. Or. Geol. 63, 13–16 (21–35).

Chadwick, O.A., Brimhall, G.H., Hendricks, D.M., 1990. From a black to a gray box — a mass balance interpretation of pedogenesis. Geomorphology 3, 369–390.

Drever, J.I., 1973. The preparation of oriented clay mineral specimens for X-ray diffraction analysis by a filter-membrane peel technique. Am. Mineral. 58, 553–554.

Ferns, M.L., McClaughry, J.D., 2013. Stratigraphy and volcanic evolution of the middle Miocene to Pliocene La Grande-Owyhee eruptive axis in eastern Oregon. In: Reidel, S.P., Camp, V.E., Ross, M.E., Wolff, J.A., Martin, B.S., Tolan, T.L., Wells, R.E. (Eds.), The Columbia River flood basalt province. Geological Society of America Special Paper 497, pp. 401–427.

Ferns, M.L., McConnell, V.S., Madin, I.P., Johnson, J.A., 2010. Geology of the upper Grande Ronde River basin, Union County, Oregon. Oregon Department of Geology and Mineral Industries Bulletin 107, scale 1:100,000.

Gallagher, T.M., Sheldon, N.D., 2013. A new paleothermometer for forest paleosols and its implications for Cenozoic climate. Geology 41, 647–650.

Gamble, E.E., Daniels, R.B., Nettleton, W.D., 1970. Geomorphic surfaces and soils in the Black Creek Valley, Johnston County, North Carolina. Soil Sci. Soc. Am. Proc. 34, 276–281.

Graham, A., 1999. Middle Eocene through Pliocene North American vegetational history: 16.3–1.6 Ma. Late Cretaceous and Cenozoic History of North American Vegetation: North of Mexico. Oxford University Press, New York, pp. 142–186.

Greenwood, D.R., 1991. The taphonomy of plant macrofossils. In: Donovan, S.K. (Ed.), The Processes of Fossilization, pp. 141–169 (Columbia, New York).

Hickson, C.J., Juras, S.J., 1986. Sample contamination by grinding. Can. Mineral. 24, 585–589.

Holbourn, A., Kuhnt, W., Schulz, M., Erlenkeuser, H., 2005. Impacts of orbital forcing and atmospheric carbon dioxide on Miocene ice-sheet expansion. Nature 438, 483–487.

Holbourn, A., Kuhnt, W., Schulz, M., Flores, J.-A., Andersen, N., 2007. Orbitally-paced climate evolution during the middle Miocene "Monterey" carbon-isotope excursion. Earth Planet Sci. Lett. 261, 534–550.

Hooper, P.R., Swanson, D.A., 1990. The Columbia River Basalt Group and associated volcanic rocks of the Blue Mountains province. In: Walker, G.W. (Ed.), Geology of the Blue Mountains Region of Oregon, Idaho, and Washington: Cenozoic Geology of the Blue Mountains Region. U. S. Geol. Surv. Prof. Pap 1437, pp. 1–37.

Howarth, R.J., 1998. Improved estimators of uncertainty in proportions, point-counting, and pass–fail test results. Am. J. Sci. 298, 594–607.

Kohn, M.J., Miselis, J.L., Fremd, T.J., 2002. Oxygen isotope evidence for progressive uplift of the Cascade Range, Oregon. Earth Planet. Sci. Lett. 204, 151–165.

Kraus, M.J., 1999. Paleosols in clastic sedimentary rocks: their geologic applications. Earth Sci. Rev. 47, 41–70.

Mack, G.H., James, W.C., Monger, H.C., 1993. Classification of paleosols. Geol. Soc. Am. Bull. 105, 129–136.

Maynard, J.B., 1992. Chemistry of modern soils as a guide to interpreting Precambrian paleosols. J. Geol. 100, 279–289.

Metzger, C.A., Retallack, G.J., 2010. Paleosol record of Neogene climate change in the Australian outback. Aust. J. Earth Sci. 57, 871–885.

Moore, D.M., Reynolds, R.C., 1997. X-Ray Diffraction and the Identification and Analysis of Clay Minerals, Second ed. Oxford University Press, New York.

Nettleton, W.D., Sleeman, J.R., 1985. Micromorphology of vertisols. In: Douglas, L.A., Thompson, M.L. (Eds.), Soil Micromorphology and Soil Classification. Soil Sci. Soc. Am. Spec. Pub 15, pp. 165–196.

Parsons, R.B., 1978. Soil–geomorphology relations in mountains of Oregon, U.S.A. Geoderma 21, 25–39.

Pierre, G., 1990. Générations d'altérites dans le Massif central Français (Auvergne, Aubrac, Vélay) du Miocène au Quaternaire: implications paléoclimatologiques et géomorphologiques. Physio-Géo 20, 31–49.

PRISM Climate Group, Oregon State University, 2012. 30-year normalsAvailable online at http://prism.oregonstate.edu (Accessed September 2014).

Reidel, S.P., Camp, V.E., Tolan, T.L., Martin, B.S., 2013. The Columbia River flood basalt province: stratigraphy, areal extent, volume, and physical volcanology. In: Reidel, S.P., Camp, V.E., Ross, M.E., Wolff, J.A., Martin, B.S., Tolan, T.L., Wells, R.E. (Eds.), The Columbia River flood basalt province. Geol. Soc. Am. Spec. Pap 497, pp. 1–43.

Retallack, G.J., 1991. Untangling the effects of burial alteration and ancient soil formation. Annu. Rev. Earth Planet. Sci. 19, 183–206.

Retallack, G.J., 1999. Postapocalyptic greenhouse paleoclimate revealed by earliest Triassic paleosols in the Sydney Basin, Australia. Geol. Soc. Am. Bull. 111, 52–70.

Retallack, G.J., 2001. A 300-million-year record of atmospheric carbon dioxide from fossil plant cuticles. Nature 411, 287–290.

Retallack, G.J., 2007. Cenozoic paleoclimate on land in North America. J. Geol. 115, 271–294.

Retallack, G.J., 2009a. Cenozoic cooling and grassland expansion in Oregon and Washington. PaleoBios 28, 89–113.

Retallack, G.J., 2009b. Refining a pedogenic-carbonate CO_2 paleobarometer to quantify a middle Miocene greenhouse spike. Palaeogeogr. Palaeoclimatol. Palaeoecol. 281, 57–65.

Retallack, G.J., Wynn, J.G., Benefit, B.R., McCrossin, M.L., 2002. Paleosols and paleoenvironments of the middle Miocene, Maboko Formation, Kenya. J. Hum. Evol. 42, 659–703.

Rice, T.J., Buol, S.W., Weed, S.B., 1985. Soil–saprolite profiles derived from mafic rocks in the North Carolina piedmont: I. Chemical, morphological, and mineralogical characteristics and transformations. Soil Sci. Soc. Am. J. 49, 171–178.

Schoeneberger, P.J., Wysocki, D., Benham, E.C., Soil Survey Staff, 2012. Field Book for Describing and Sampling Soils. Natural Resources Conservation Service, Lincoln.

Shaw, J.N., West, L.T., Hajek, B.F., 2001. Ca–Mg ratios for evaluating pedogenesis in the piedmont province of the southeastern United States of America. Can. J. Soil Sci. 81, 415–421.

Sheldon, N.D., 2003. Pedogenesis and geochemical alteration of the Picture Gorge subgroup, Columbia River basalt, Oregon. Geol. Soc. Am. Bull. 115, 1377–1387.

Sheldon, N.D., 2006. Using paleosols of the picture Gorge Basalt to reconstruct the middle Miocene climatic optimum. PaleoBios 26, 27–36.

Sheldon, N.D., Retallack, G.J., 2001. Equation for compaction of paleosols due to burial. Geology 29, 247–250.

Sheldon, N.D., Retallack, G.J., 2004. Regional paleoprecipitation records from the late Eocene and Oligocene of North America. J. Geol. 112, 487–494.

Sheldon, N.D., Tabor, N.J., 2009. Quantitative paleoenvironmental and paleoclimatic reconstruction using paleosols. Earth Sci. Rev. 95, 1–52.

Sheldon, N.D., Tabor, N.J., 2013. Using paleosols to understand paleo-carbon burial. In: Driese, S., Nordt, L. (Eds.), New Frontiers in Paleopedology and Terrestrial Paleoclimatology. SEPM Special Publication 104, pp. 71–78.

Sheldon, N.D., Retallack, G.J., Tanaka, S., 2002. Geochemical climofunctions from North American soils and application to paleosols across the Eocene–Oligocene boundary in Oregon. J. Geol. 110, 687–696.

Smith, B.J., McAlister, J.J., 1995. Mineralogy, chemistry and palaeoenvironmental significance of an Early Tertiary Terra Rossa from Northern Ireland: a preliminary review. Geomorphology 12, 63–73.
Soil Survey Staff, 2003. Web Soil Survey. USDA-Natural Resources Conservation Service, (Available online at http://websoilsurvey.nrcs.usda.gov/. Accessed September 2014).
Soil Survey Staff, 2014. Keys to Soil Taxonomy, Twelfth ed. USDA-Natural Resources Conservation Service, Washington, DC.
Stiles, C.A., Mora, C.I., Driese, S.G., 2003. Pedogenic processes and domain boundaries in a Vertisol climosequence: evidence from titanium and zirconium distribution and morphology. Geoderma 116, 279–299.
Stoops, G., 2003. Guidelines for Analysis and Description of Soil and Regolith Thin Sections. Soil Science Society of America, Madison, Wisconsin.
Takeuchi, A., Larson, P.B., 2005. Oxygen isotope evidence for the late Cenozoic development of an orographic rain shadow in eastern Washington, USA. Geology 33, 313–316.
Takeuchi, A., Larson, P.B., Suzuki, K., 2007. Influence of paleorelief on the mid-Miocene climate variation in southeastern Washington, northeastern Oregon, and western Idaho, USA. Palaeogeogr. Palaeoclimatol. Palaeoecol. 254, 462–476.
U.S. Energy Research and Development Administration, 1976. Preliminary Feasibility Study on Storage of Radioactive Wastes in Columbia River Basalts: U.S. Energy Research and Engineering Division Report ARH-ST-137 under contract E(45–1)-2130, (183 pp.).
Wolfe, J.A., 1993. A method of obtaining climatic parameters from leaf assemblages. U.S. Geol. Surv. Bull. 2040.
Wolfe, J.A., Schorn, H.E., Forest, C.E., Molnar, P., 1997. Paleobotanical evidence for high altitudes in Nevada during the Miocene. Science 276, 1672–1675.
Yang, J., Wang, Y.-F., Spicer, R.A., Mosbrugger, V., Li, C.-S., Sun, Q.-G., 2007. Climatic reconstruction at the Miocene Shanwang basin, China, using leaf margin analysis, CLAMP, coexistence approach, and overlapping distribution analysis. Am. J. Bot. 94, 599–608.
Zachos, J., Pagani, M., Sloan, L., Thomas, E., Billups, K., 2001. Trends, rhythms, and aberrations in global climate 65 Ma to present. Science 292, 686–693.
Zhang, M., Karathanasis, A.D., 1997. Characterization of iron–manganese concretions in Kentucky Alfisols with perched water tables. Clays Clay Miner. 45, 428–439.